Wake transition in the flow around two circular cylinders in staggered arrangements

Bruno CARMO, Spencer SHERWIN, Peter BEARMAN, Richard WILLDEN

Imperial College London - Department of Aeronautics.

South Kensington Campus, London - UK. SW7 2AZ.

Abstract. This work focuses on the wake transition of the flow around two circular cylinders when placed in staggered arrangements with a fixed streamwise separation of $5D$ and varying the cross stream separation from $0D$ to $3D$. The wake transition is compared to that of a single isolated cylinder. Linear stability analysis, utilising Floquet theory, and direct numerical simulations, using the spectral/hp element method, are carried out. It is found that besides modes A and B, mode C can also appear in the wake transition, depending on the relative positioning of the cylinders. The structure of mode C is analysed and the non-linear character of the bifurcation for this mode is investigated.

Key words: Wake transition, bluff bodies, flow interference.

1. Introduction

The flow around circular cylinders has been extensively studied due to its practical importance in engineering and scientific relevance in fluid mechanics. In the last two decades, much effort has been focused on the study of the three-dimensional transition that takes place in the von Kármán wake that appears in the flow downstream of a single cylinder. This line of research in its contemporary form was instigated by the seminal work of Williamson [15], in which the two fundamental three-dimensional instabilities that occur in the wake transition, modes A and B, were first identified. A great leap forward occurred with the work of Barkley and Henderson [2], who performed high accuracy Floquet stability analyses of two-dimensional time periodic base flows, precisely identifying the critical Reynolds numbers and also characterising each of the modes that take part in the wake transition. The non-linear characterisation of the modes was later investigated in a number of works using direct numerical simulations, for example [6] and [5]. When some degree of asymmetry is introduced in the configuration, a period-doubling mode, which is commonly called mode C, is also found in the wake transition. As far as we are aware, the first evidence of this mode, appeared in the computations and experiments of Zhang et al. [16] when a tiny trip wire was placed close to a circular cylinder. More recently the same mode was identified in the flow around bluff rings [11, 12, 13].

Another important aspect of the flow around bluff bodies such as circular cylinders is that the flow field and fluid loads change dramatically when compared to the flow around an isolated body if two or more bodies are placed in close proximity in the fluid stream. Here we deal with the case of circular cylinders in staggered

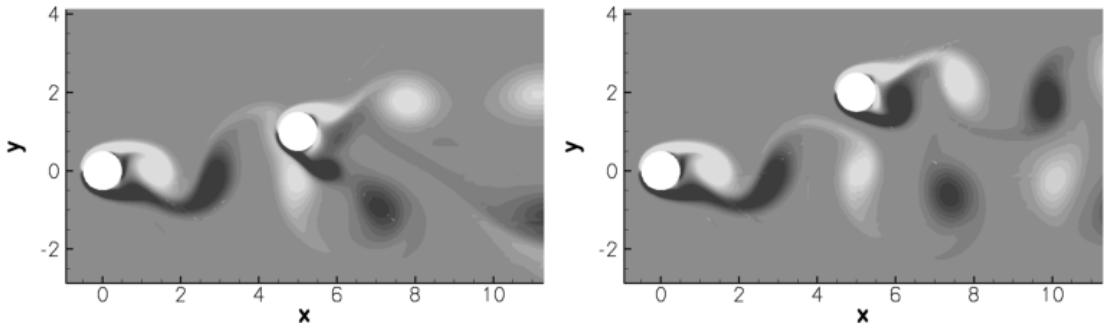

(a) $L_y = 1.0$ (b) $L_y = 2.0$

Figure 1: Instantaneous vorticity contours, flow around staggered arrangements, $Re = 200$, two-dimensional simulations. Light contours represent regions of negative vorticity and dark contours represent regions of positive vorticity.

arrangements, as illustrated in figure 1. Sumner et al. [14] put forward a taxonomy for the flow regimes observed in their experiments with such arrangements. This work was extended by Akbari and Price [1], who reproduced the flow regimes using computational simulations and scrutinised the physical features observed in each. As far as we are aware, no computational work addressing the three-dimensional aspects of the flow around staggered arrangements of circular cylinders has yet been published. This paper focus on the changes that occur in the transition in the wake when the flow around staggered arrangements is compared to the flow around a single cylinder. By means of linear stability analysis of two-dimensional periodic base flows and also fully three-dimensional simulations, the instabilities that arise at the beginning of the transition are characterised.

2. Overview

The methodology adopted in this investigation can be divided into three distinct parts: two-dimensional simulations, Floquet stability analysis and three-dimensional simulations. In the next three subsections, an overview of the mathematical formulation and computational implementation of each of these parts is provided.

2.1. Two-dimensional base flow calculation

We consider a two-dimensional incompressible viscous flow, which is governed by the Navier-Stokes equations. These equations can be written in non-dimensional form using the cylinder diameter as the reference length and the free-stream flow speed U_∞ as the reference speed:

$$\frac{\partial \mathbf{u}}{\partial t} = -(\mathbf{u}.\nabla)\mathbf{u} - \nabla p + \frac{1}{Re}\nabla^2\mathbf{u}, \tag{1}$$

$$\nabla.\mathbf{u} = 0, \tag{2}$$

where $\mathbf{u} \equiv (u, v, w)$ is the velocity field, t is the time, p is the static pressure and Re is the Reynolds number. The pressure is assumed to be scaled by the constant density ρ. These equations were discretized following the Spectral/hp method as described in [9]. To generate the base flows, equations (1) and (2) were solved in two dimensions, using a stiffly stable splitting scheme, following [8].

2.2. Floquet stability analysis

We considered periodic two-dimensional base flows $\mathbf{U}(x, y, t)$, with period T, and checked their stability with respect to an infinitesimal three-dimensional perturbation $\mathbf{u}'(x, y, z, t)$. The equations that govern the perturbation evolution to leading order are the linearized Navier-Stokes equations:

$$\frac{\partial \mathbf{u}'}{\partial t} = -(\mathbf{U}.\nabla)\mathbf{u}' - (\mathbf{u}'.\nabla)\mathbf{U} - \nabla p' + \frac{1}{Re}\nabla^2\mathbf{u}', \tag{3}$$

$$\nabla.\mathbf{u}' = 0, \tag{4}$$

where $p'(x, y, z, t)$ is the pressure perturbation. The velocity boundary conditions that were imposed on this system are $u' = 0$ on boundaries where Dirichlet conditions are specified for the base flow, and $\partial u'/\partial n = 0$ on boundaries where Neumann conditions are specified for the base flow.

The right hand side of (3), subjected to the incompressibility constraint of equation (4), can be represented by a linear operator $\mathbf{L}(\mathbf{u}')$, which is T-periodic because it depends on the base flow $\mathbf{U}(x, y, t)$, which is T-periodic. Therefore, the stability of the system can be investigated using Floquet analysis [2]. The solutions of the system can be decomposed into a sum of solutions of the form $\tilde{\mathbf{u}}(x, y, z, t)e^{\sigma t}$, where $\tilde{\mathbf{u}}(x, y, z, t)$, which are called Floquet modes, are T-periodic solutions. The complex exponents σ are the Floquet exponents, and the sign of their real parts determines the stability of the system. However, in Floquet type problems it is more usual to consider the Floquet multiplier $\mu \equiv e^{\sigma T}$ instead of the Floquet exponent. If the Floquet multiplier is located inside the unit circle ($|\mu| < 1$), then the solution will decay exponentially with time, and if the multiplier is located outside the unit circle ($|\mu| > 1$), the solution will grow exponentially with time, and the system is therefore unstable.

If we consider a system that is homogeneous in the spanwise direction z, a further simplification can be made. A perturbation of the velocity field can be expressed in terms of the Fourier integral:

$$\mathbf{u}'(x, y, z, t) = \int_{-\infty}^{\infty} \hat{\mathbf{u}}(x, y, \beta, t)e^{i\beta z}d\beta \tag{5}$$

and similarly for p'. Since equations (3) and (4) are linear, modes with different β do not couple. As the velocity components $(\hat{u}, \hat{v}, \hat{w})$ and pressure $\hat{p}$ depend only on x, y and t, the three-dimensional stability problem can be reduced to a series of two-dimensional stability problems, each with a different value of β. Consequently, the stability of such two-dimensional incompressible periodic flows in respect to three-dimensional perturbations can be analysed by computing the Floquet multipliers and corresponding modes as a function of Re and β.

2.3. Three-dimensional simulations and non-linear characterisation of the transition

The three-dimensional computational calculations utilised the same framework outlined in section 2.1. However, the spanwise direction was treated using a Fourier expansion discretization [7]. The three-dimensional simulation results enabled a non-linear analysis of the transitions to be conducted. The Landau equation has often been successfully used in hydrodynamics as a low dimensional model to describe

the non-linear behaviour of transitions close to their respective critical points see for example [12, 5]. Here, the Landau equation is written up to third order, using the same notation as in [12]:

$$\frac{dA}{dt} = (\sigma + i\omega)\, A - l\,(1 + ic)\,|A|^2 A + \ldots, \tag{6}$$

where $A(t)$ is the complex amplitude of the perturbation mode being considered. The term $(\sigma + i\omega)$ in (6) is the eigenvalue obtained from the linear stability analysis, and in the present case is the Floquet exponent. The parameter l is the real part of the third order coefficient and the classification of the transition depends directly on its sign. If $l > 0$, the transition is supercritical. On the other hand, if $l < 0$, the transition is said to be subcritical. Lastly, c is called the Landau constant and it modifies the oscillation frequency at saturation. The value of the amplitude A was calculated as in [5].

3. Numerical simulations

Figure 1 shows the geometry investigated in this research. The two cylinders have the same diameter D. For all cases, the streamwise distance between the centres of the cylinders, L_x, is $5.0D$. The transversal distances tested, L_y, were $0.0D$, $0.5D$, $1.0D$, $2.0D$, $2.5D$ and $3.0D$. Calculations were also carried out for the single cylinder case, which served as a benchmark for comparison with the two-cylinder cases. The Reynolds numbers simulated were 200, 250, 300 and 350, covering the wake transition range for the flow around a single cylinder.
8th-degree polynomials expansions were used as basis functions for the spatial discretization, and the integration in time was second-order accurate. The value of the non-dimensional time-step varied from 0.006 to 0.004, depending only on Re. Uniform stream velocity boundary conditions ($u = 1$, $v = 0$) were imposed at the upstream boundary and upper and lower surfaces of the computational domain. At the cylinder walls, a no-slip condition ($u = 0$, $v = 0$) was imposed. Finally, at the downstream border, Newmann boundary conditions ($\partial u/\partial \mathbf{n} = 0, \partial v/\partial \mathbf{n} = 0$) were applied. For the three-dimensional simulations, periodic boundary conditions were set on the boundary planes located at the extreme values of z. We used 8 Fourier modes (16 planes) in the z direction.
For all stability calculations, the calculations spanned wave numbers (β) from 0.0 to 15.0. The calculations were carried out until the residual of the biggest eigenvalue reached a value less than 10^{-5}.
In the remainder of this paper, all the distances will be given in diameters.

4. Results

4.1. Floquet stability calculations

Single cylinder

The values of the Floquet multiplier, μ, for the stability calculations of the flow around a single cylinder are shown in figure 2, and they compare well with those presented in [2]. Two different unstable modes, called modes A and B, are present

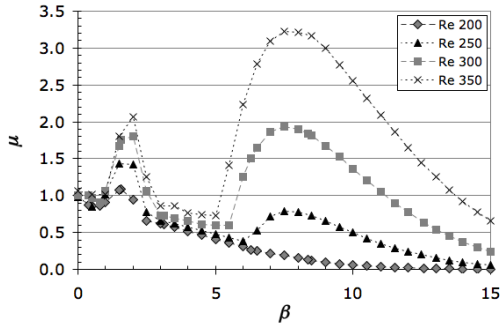

Figure 2: Floquet multiplier μ as a function of the spanwise wavenumber β for various Re. Flow around a single cylinder.

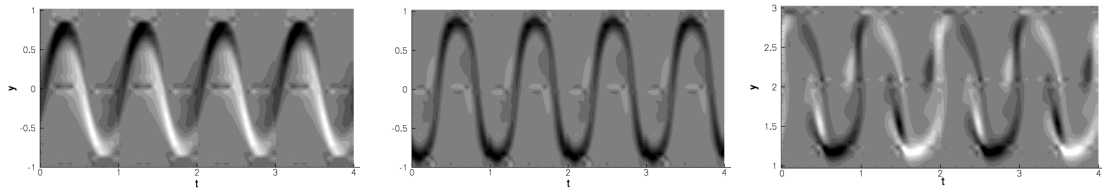

(a) Mode A – $Re = 200$, $\beta = 1.571$ (b) Mode B – $Re = 300$, $\beta = 7.500$ (c) Mode C – $Re = 300$, $\beta = 1.571$

Figure 3: x-vorticity of the unstable eigenvector. (a) and (b) - flow around a single cylinder, data extracted from line $x = 2.0$; (c) - flow around a staggered arrangement with $L_y = 2.0$, data extracted from line $x = 7.0$. Light regions correspond to negative and dark to positive streamwise vorticity of the eigenvector. Time is non-dimensionalized using the shedding period.

in the Re range considered. Mode A, which corresponds to the peaks of lowest β in each of the curves exposed in figure 2, is the first to appear in terms of Re, and is already unstable for $Re = 200$. For this mode, the wavelength of maximum growth rate is around $4.0D$. Mode B corresponds to the peak of higher β in the curves shown in the graph, having a wavelength of maximum growth rate of about $0.8D$, and, among the cases calculated, it is only unstable for $Re = 300$ and $Re = 350$.
An important difference between modes A and B is their spatio-temporal symmetries [2, 4]. In figures 3a and 3b streamwise vorticity contours evaluated in time on a vertical line $2D$ downstream of the cylinder are presented. For mode A, the vorticity has different sign either side of the wake centreline, for mode B, the vorticity has the same sign throughout the cycle.

Staggered Arrangements

Figure 1 shows examples of instantaneous vorticity contours of the two-dimensional base flows for staggered arrangements. For low cross stream separations, $L_y \leqslant 1.0$, a single wide wake was observed downstream of the arrangement, while for higher separations, $L_y \geqslant 2.0$, two distinct wakes were observed. For all cases with two cylinders two shedding periods T were considered in the stability calculations, in order to take into account the vortex interaction that happens in the far wake, which was found to have $2T$-periodicity.
For $L_y = 0.0$ and 0.5, the shape of the curves μ *versus* β were very similar to the

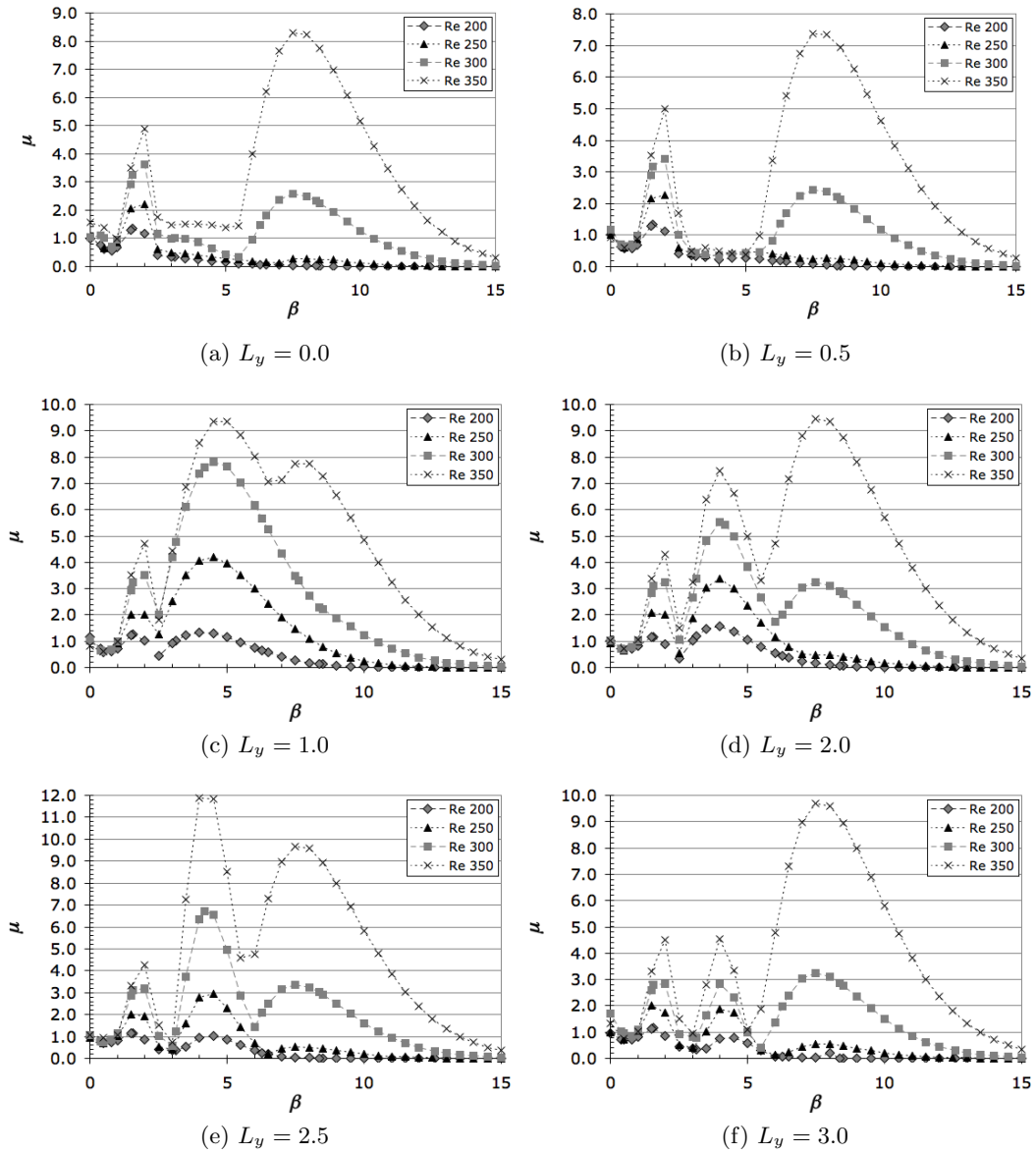

(a) $L_y = 0.0$ (b) $L_y = 0.5$

(c) $L_y = 1.0$ (d) $L_y = 2.0$

(e) $L_y = 2.5$ (f) $L_y = 3.0$

Figure 4: Floquet multiplier μ as a function of the spanwise wavenumber β for various Re. Staggered arrangements.

single cylinder case, as can be seen in figures 4a and 4b. The two peaks, one for mode A and one for mode B, are clearly evident.

In order to examine the structure of the modes in greater detail, figure 5 shows streamwise vorticity contours of the unstable eigenvectors. Figure 5a shows structures characteristics of mode A. Of note is that the instability first develops in the near wake of the upstream cylinder, but then grows stronger when it reaches the downstream cylinder. Also of note is the higher energy in the region of vortex interaction far downstream. It seems that the vortex merging that occurs in this region helps to reinforce mode A structures. The results are different for mode B. In figure 5b, we see that the instability first develops in the near wake of the upstream cylinder, as in the mode A case. However, the streamwise vortical structures do not seem to gain significant strength when they impinge upon the downstream cylin-

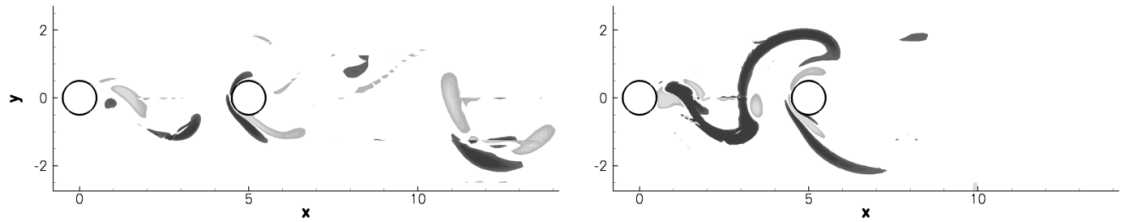

(a) $\beta = 1.571$ (b) $\beta = 7.500$

Figure 5: x-vorticity of eigenvectors, flow around two cylinders with $L_y = 0.0$, $Re = 300$. Dark contours correspond to positive x-vorticity and light contours to negative x-vorticity.

Table 1: Critical Re for modes A (Re_A), B (Re_B) and C (Re_C) and mode C bifurcation type. The Reynolds numbers for which the wake first becomes 3-D in each configuration are written in bold face.

L_y	Re_A	Re_B	Re_C	*Mode C bifurcation type*
$1.0D$	**183**	N/A	191	subcritical
$2.0D$	190	N/A	**178**	supercritical
$2.5D$	**192**	264	198	supercritical
$3.0D$	**193**	263	209	subcritical
Single cylinder [2]	**188.5**	259	–	–

der. Also, no mode B structures were observed in the vortex interaction region far downstream.

For $L_y = 1.0$, the transition deviated from that observed for the flow around a single cylinder. A peak of intermediate wave number dominates, as can be seen in figure 4c. This corresponds to the asymmetric period-doubling mode C, which will be described and analysed in more detail in section 4.2. The peak relating to mode B is only visible for $Re = 350$, nevertheless it was verified that this mode is already unstable for $Re = 300$, but that the correspondent Floquet multiplier is smaller than that relating to mode C. Table 1 shows that the critical Reynolds number for which mode A became unstable was lower than for a single cylinder. Mode C became unstable for $Re_C = 191$ and the instability had a wavelength $L_{zC} = 1.55$.

For configurations in which two distinct wakes could be observed ($2.0 \leqslant L_y \leqslant 3.0$), mode C was also detected. Figures 4d, 4e and 4f exhibit three distinct peaks, and the peak relating to mode C appears in a region of intermediate wave numbers between the peaks associated with modes A and B. For the three cases, mode A bifurcates at a slightly higher Re than it does in the single cylinder case and the same trend is observed for the mode B bifurcation (see table 1). However, as shown in table 1, as L_y increases mode C becomes unstable at a progressively increasing Re. This behaviour is not surprising, given that the larger the distance between the cylinders, the closer the flow is to the single cylinder case, for which no mode C instability is observed.

4.2. Mode C

In this section, the intermediate wave number mode that appears in the wake transition for $L_y \geqslant 1.0$ is examined. This mode is in fact a mode C instability [16, 11],

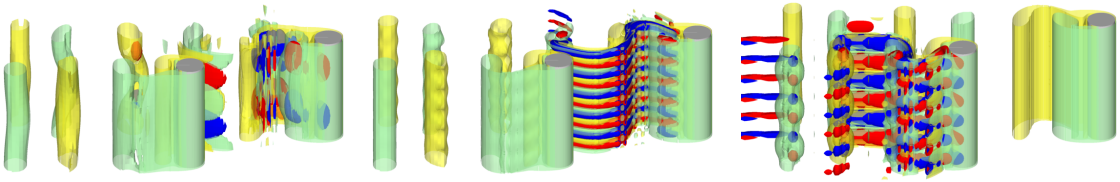

(a) Mode A, $L_z = 4.000$ (b) Mode B, $L_z = 0.838$ (c) Mode C, $L_z = 1.571$

Figure 6: Three-dimensional structures of the instability modes, configuration $L_y = 2.0$, $Re = 300$. The represented flow fields are linear combinations of the base-flow and the unstable Floquet mode. Translucent green and yellow surfaces are iso-surfaces of negative and positive ω_z, respectively. Solid blue and red surfaces are iso-surfaces of negative and positive ω_x respectively. Flow is from right to left.

as will be shown later, so this designation will be used from now on. A significant difference between this mode and modes A and B is that mode C appears in the near wake of the downstream cylinder, while modes A and B originate in the near wake of the upstream cylinder, as can be seen in figure 6. When considering only one shedding period T in the instability calculations, the results gave real negative Floquet multipliers. Hence this is a period-doubling mode, just like the mode C instability reported by [11].

Figure 3c shows the time history of the x-vorticity contours of the eigenvector of mode C on a vertical line $2D$ aft of the downstream cylinder ($7D$ aft of the upstream cylinder). The first important aspect to notice is that this mode is not symmetric in relation to the wake centreline (in figure 3c, the wake centreline is $y = 2.0$). A second aspect of note is that this mode has a period of $2T$ in contrast with modes A and B, which are T-periodic.

Figure 6 shows plots of vorticity iso-surfaces of the base flow combined with the unstable Floquet mode for modes A, B and C. The three-dimensional structures of modes A and B are very similar to those observed in the flow around a single cylinder [5]. For mode A, the streamwise vorticity is stronger in the primary vortex cores, whereas for mode B it is stronger in the braid shear layers. Apart from the different wavelength and its period-doubling nature, mode C presents a structure similar to mode B, in the sense that it is stronger in the braid shear layers, although bubbles of non-negligible stream wise vorticity are also observed in the primary vortex cores. The asymmetrical nature of mode C is also clear in the figure, as the stronger streamwise vorticity is observed in the side of the wake closer to the vortex street formed from the upstream cylinder.

As previously mentioned, the period-doubling mode C was also identified by [11], in stability calculations of the flow around bluff rings with aspect ratio (ratio between the ring diameter and the cross section diameter) greater than 4.0. In this work they found a maximum growth rate for mode C for spanwise wavelengths between $1.6D$ and $1.7D$, which agrees well with the results of the present investigation. Furthermore, striking similarities between the three-dimensional structure of mode C are found when comparing figure 6 to the results presented in [12]. The mode C wavelength found in the present results is also reasonably close to the value of $1.8D$ reported in [16]. In this study, mode C appeared in their experiments when a thin control wire was placed near the cylinder, and they reproduced this result in computational simulations by enforcing zero velocity in the point of the mesh

that corresponded to the coordinate of the centre of the control wire. We note that asymmetry is again involved in the base flow.

4.3. Non-linear analysis

In order to investigate the non-linear evolution of mode C, fully three-dimensional simulations were also performed. The configurations $L_y = 1.0$, $L_y = 2.0$, $L_y = 2.5$ and $L_y = 3.0$ were tested, and Reynolds numbers slightly higher than critical Re for mode C bifurcation (Re_c) for each configuration were selected. For each case, the periodic span of the domain was the wavelength of the mode C instability at its onset and the growth and saturation of the infinitesimal perturbation were observed. By plotting graphs of $d[\ln(A)]/dt$ against $|A|^2$, as in [12], and comparing the growth predicted by the linear stability results to the actual growth observed in the simulations, we could characterise the bifurcation type for mode C in each of the configurations.
The rightmost column of table 1 shows the results of the non-linear analysis. Mode C bifurcation is subcritical for $L_y = 1.0$, supercritical for $L_y = 2.0$ and $L_y = 2.5$ and again subcritical for $L_y = 3.0$. However, since the vortex shedding regime for $L_y = 1.0$ is different from that for $L_y \geqslant 2.0$, the configuration $L_y = 1.0$ must be considered separately if we want to isolate the three-dimensional effects.
For configurations $L_y = 2.0$ and $L_y = 2.5$ mode C presented a supercritical character, but it bifurcated before mode A for $L_y = 2.0$ and after mode A for $L_y = 2.5$. For $L_y = 3.0$, it bifurcated after mode A, but through a subcritical route. As far as we are aware, this is the first time it is reported that when mode C become unstable after mode A, it can be done through either a supercritical or a subcritical route, depending on the geometry. To the best of our knowledge, the only publication that addressed a non-linear analysis of mode C transition was [12], and the mode C bifurcations reported there are either supercritical and before mode A or subcritical and after mode A.

5. Conclusion

The basic modes in the wake transition in the flow around a single circular cylinder, modes A and B, were also found in the staggered arrangements considered in this investigation. This enforces the thesis that these modes are fundamental in the transition to turbulence in vortex wakes, even in the case of multiple cylinders.
Another important finding of this study was the presence of mode C in the wake transition for some asymmetrical arrangements. The linear stability results for this mode agree well with previous investigations [11, 16] in many aspects, such as type of perturbation symmetry, wavelength and periodicity. Interestingly, while modes A and B appear in the near wake of the upstream cylinder, while mode C appears in the near wake of the downstream cylinder. The non-linear analysis showed that mode C can bifurcate through either a subcritical or a supercritical route, depending on L_y, and the character of this bifurcation is not directly related to order the modes bifurcate.
For $L_y \geqslant 1.0$, all three modes appear in the Re range investigated, and the fact that mode C appears for $L_y = 1.0$ and for $L_y \geqslant 2.0$ indicates that the vortex shedding regime and the presence of mode C are not directly related, although both depend

on the geometrical configuration of the bodies. In addition, the fact that mode C appeared for two substantially different wakes ($L_y = 1.0$ and $L_y \geqslant 2.0$) corroborates the thesis that mode C is a fundamental mode in the transition of time-periodic wakes with a certain degree of Z_2 asymmetry [11, 12]. This mode seems to replace the quasi-periodic mode that emerges in Z_2 symmetric wakes [3, 10], spanning the same wave number range.

References

[1] M. H. Akbari and S. J. Price. Numerical investigation of flow patterns for staggered cylinder pairs in cross-flow. *Journal of Fluids and Structures*, 20:533–554, 2005.

[2] D. Barkley and R. D. Henderson. Three-dimensional floquet stability analysis of the wake of a circular cylinder. *Journal of Fluid Mechanics*, 322:215–241, 1996.

[3] H. M. Blackburn and J. M. Lopez. On three-dimensional quasiperiodic floquet instabilities of two-dimensional bluff body wakes. *Physics of Fluids*, 15(8):57–60, 2003.

[4] H. M. Blackburn, F. Marques, and J. M. Lopez. Symmetry breaking of two-dimensional time-periodic wakes. *Journal of Fluid Mechanics*, 522:395–411, 2005.

[5] R. D. Henderson. Nonlinear dynamics and pattern formation in turbulent wake transition. *Journal of Fluid Mechanics*, 352:65–112, 1997.

[6] R. D. Henderson and D. Barkley. Secondary instability of the wake of a circular cylinder. *Physics of Fluids*, 8(6):1683–1685, June 1996.

[7] G. E. Karniadakis. Spectral element-fourier methods for incompressible turbulent flows. *Computer Methods in Applied Mechanics and Engineering*, 80:367–380, 1990.

[8] G. E. Karniadakis, M. Israeli, and S. A. Orszag. High-order splitting methods for the incompressible navier-stokes equations. *Journal of Computational Physics*, 97:414–443, 1991.

[9] G. E. Karniadakis and S. J. Sherwin. *Spectral/hp Element Methods for Computational Fluid Dynamics*. Oxford University Press, 2nd edition, 2005.

[10] F. Marques, J. M. Lopez, and H. M. Blackburn. Bifurcations in systems with z2 spatio-temporal and o(2) spatial symmetry. *Physica D*, 189:247–276, 2004.

[11] G. J. Sheard, M. C. Thompson, and K. Hourigan. From spheres to circular cylinders: the stability and flow structures of bluff ring wakes. *Journal of Fluid Mechanics*, 492:147–180, 2003.

[12] G. J. Sheard, M. C. Thompson, and K. Hourigan. From spheres to circular cylinders: non-axisymmetric transitions in the flow past rings. *Journal of Fluid Mechanics*, 506:45–78, 2004.

[13] G. J. Sheard, M. C. Thompson, and K. Hourigan. Subharmonic mechanism of the mode c instability. *Physics of Fluids*, 17(11):Art. No. 111702, 2005.

[14] D. Sumner, S. J. Price, and M. P. Païdoussis. Flow-pattern identification for two staggered circular cylinders in cross-flow. *Journal of Fluid Mechanics*, 411:263–303, 2000.

[15] C. H. K. Williamson. The existence of two stages in the transition to three-dimensionality of a cylinder wake. *Physics of Fluids*, 31(11):3165–3168, 1988.

[16] H.-Q. Zhang, U. Fey, B. R. Noack, M. König, and H. Eckelmann. On the transition of the cylinder wake. *Physics of Fluids*, 7(4):779–794, 1995.